Laminar-turbulent intermittency in pipe flow for an Herschel-Bulkley fluid: Radial receptivity to finite-amplitude perturbations

Antoine Charles,[1] Francesco Romanò,[2] Thierry Ribeiro,[3] Sam Azimi,[4] Vincent Rocher,[4] Jean-Christophe Baudez,[1] and S. Amir Bahrani[1, a)]

[1)] *IMT Nord Europe, Institut Mines Télécom, Univ. Lille, Center for Energy and Environment, F-59000 Lille, France.*

[2)] *Univ. Lille, CNRS, ONERA, Arts et Métiers Institute of Technology, Centrale Lille, FRE 2017-LMFL-Laboratoire de Mécanique des Fluides de Lille - Kampé de Fériet, F-59000, Lille, France.*

[3)] *Institut Polytechnique UniLaSalle, Université d'Artois, ULR 7519, 19 rue Pierre Waguet, 60000 Beauvais*

[4)] *SIAAP - Service public pour l'assainissement francilien, Direction Innovation, 82 avenue Kléber, 92700 Colombes*

(Dated: 30 October 2023)

We investigate the laminar-to-turbulent transition for non-Newtonian Herschel-Bulkley (HB) fluids that exhibit either a shear-thinning or a shear-thickening behavior. The reduced-order model developed in this study also includes the effect of yield-stress for the fluid. Within our model framework, we investigate how the Newtonian dynamics change when significant non-Newtonian effects are considered either via the flow index n, or the yield-stress τ_0, or both. We find that an increase of τ_0, as well as a decrease of n lead to a delayed transition if a perturbation of given turbulent intensity is injected at various radial locations. As the radial position of the injection for the perturbation is varied in this study, our reduced-order model allows for the investigation of the flow receptivity to the finite-amplitude perturbations and to their radial position of inception. We observe that, for a given mean flow profile, the same perturbation becomes more prone to induce turbulence the closer it approaches the wall because of its initial amplitude being relatively higher with respect to the local mean flow. An opposite trend is found when the perturbation amplitude is rescaled on the local mean flow.

The inertial Newtonian transition to turbulence in cylindrical pipe flow is one of the most studied fundamental topics of fluid mechanics (see Hof et al.[1], Faisst and Eckhardt[2], Kerswell[3] and Avila et al.[4]). There is a strong operational interest in understanding the transition to turbulence in cylindrical pipe flows, in particular to identify the relevant critical conditions that control the flow because the shear stress at the pipe wall depends on the flow regime (see Jimènez[?]). As the Hagen-Poiseuille flow is linearly stable, finite-amplitude perturbations are essential to trigger turbulence in Newtonian pipe flows. The necessary amplitude A of these perturbations has been shown to be dependent on the bulk Reynolds number Re as a power-law with an exponent between -1.5 and -1, i.e. $A \sim \mathrm{Re}^{\alpha}$ for $\alpha \in [-1.5\ ,\ -1]$ (see Hof et al.[6] and Peixinho[7]). When reaching the transitional regime, spatial and temporal switches between the laminar and the turbulent states are observed in pipe flow. This phenomenon is called intermittency and it comes from the two-states nature of pipe flow. Such systems where two stable or meta-stable points coexist are called bi-stable systems. Different flow regimes can therefore be identified: (i) a *fully-laminar regime* where no turbulent structures can be sustained and introducing a small finite-amplitude perturbation will cause locally the emergence of a turbulent puff which will necessarily decay over time, (ii) an *intermittent regime* where puffs due to the introduction of a finite-amplitude perturbation will eventually not decay and can even split into multiple puffs, and (iii) a *fully-turbulent regime* where the introduction of a finite-amplitude perturbation will cause the emergence of a slug, i.e. a sustained structure which can potentially expand in the whole pipe. These structures have been shown by Willis and Kerswell[8] using Direct Numerical Simulations (DNS) and have been confirmed experimentally by Hof et al.[9]. Their dynamics has also been studied using DNS by Song et al.[10] and their results consolidate this description. Barkley[11] developed a minimal model to explain the instability based on the interaction between the two stable states. This model qualitatively matched the DNS results and could therefore be used to interpret the path of transition to turbulence in connection with percolation theory for the perturbation (see Lemoult et al.[12]), from the decay of the puff at low Re to the strong slug at high Re. This model has recently been generalized by Romanò et al.[13] to integrate the power-law behaviour of a non-Newtonian fluid of the Ostwald type and the thermal effects on the fluid. It shows a net destabilization effect for uniformly heated walls and a nontrivial stabilizing effect for differentially heated walls, as well as a clear stabilization with an increase in the power-law index n for a power-law fluid.

In many applications, the fluids in use are complex and non-Newtonian, from concretes, cosmetics or gels to biological fluid such as blood, mucus or sludge (see Coussot[14]). In order to carry out a representative case

[a)] Electronic mail: amir.bahrani@imt-nord-europe.fr

study, the rheological parameters are selected in accordance with experimental measurements carried out on a study fluid at the IMT laboratory, i.e. digested sludge from a wastewater treatment plant. These biological fluids are shear-thinning and posses a yield-stress. They can be described by the HB model, integrating the power-law variation with the fluid yield stress:

$$\begin{cases} \tau = \tau_0 + K\dot{\gamma}^n & \tau \geq \tau_0 \\ \dot{\gamma} = 0 & \tau < \tau_0 \end{cases} \tag{1}$$

where τ is the shear stress (Pa), τ_0 the yield stress (Pa), K the consistency factor (Pa s), n the flow index $(-)$ leading to shear-thinning fluids for $n < 1$ and shear-thickening ones for $n > 1$, $\dot{\gamma}$ the shear rate (s^{-1}), R the pipe radius (m). The control parameter for the rheology of such fluids is the Herschel-Bulkley number Hb that compares the rheological properties of the fluid with the flow inertia:

$$\mathrm{Hb} = \frac{\tau_0 R^n}{K {U_0}^n} \tag{2}$$

Figure 1 shows the flow curves obtained from coaxial cylinder geometries (CC27 and CC38) placed in a rheometer, in which the inner cylinder is rotating and the external cylinder is at rest. The temperature of the external cylinder is kept fixed at 20°C. The rheological parameters τ_0, K, n derived from their fit (lines in fig. 1) by the HB model are given in the legend of fig. 1.

The onset of turbulence for a non-Newtonian fluid is impacted by the inertial characteristics of the flow (control parameter Re, just as for a Newtonian fluid), but also by the interaction of the rheological characteristics of the complex fluid with the flow. This so-called rheo-inertial transition results in a *turbulent pre-transition regime* and the asymmetry of the velocity profiles in this regime. The work of Escudier et al.[15] and Bahrani and Nouar[16] shows the existence of this regime, non-existent in Newtonian fluids, before the regime where the turbulent puffs appear. Its origin comes from the interaction between the inertia and the non-linear dependence of the viscosity with the stress. The friction coefficient C_f is then above the laminar solution described by Poiseuille's law, but below the turbulent solution predicted by Prandtl-Karman's law (see Virk[17]). The corresponding drag reduction relies on the decrease of the turbulence level due to the rheological nature of the fluid (see Escudier et al.[18]).

By linear analysis, Chekila[19] showed an increase in the critical Reynolds number Re_c for shear-thinning fluids. Such a transition delay is caused by a reduction in the energy exchange between the basic flow and the disturbance of the critical layer. By weakly non-linear stability analysis, he shows that shear-thinning behavior has a stabilising effect by stratification of the effective viscosity for a shear-thinning fluid following a Carreau model. This result suggests a delay in the transition to turbulence caused by the rheological nature of the fluid. Romanò

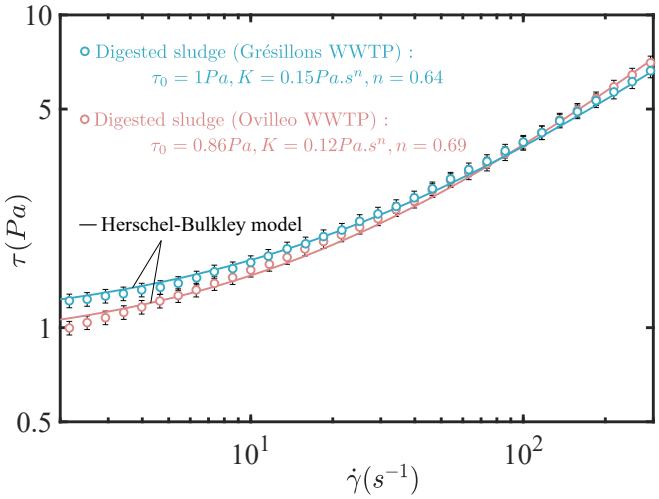

FIG. 1. Physical calibration of the HB-model parameters from the rheological curves extracted on digested sludges. Lines correspond to HB model fits. Error bars are shown in black behind the experimental points. HB parameters are specified in the legend in the top left corner. The fluid samples are digested sludge from wastewater treatment plant (WWTP) collected in the Seine Grésillons (Paris, France) WWTP and Ovilleo (Lille, France) WWTP. Further experiments (not shown) have confirmed the parameters of our fits by HB model, as well as the presence of a yield stress for both considered fluids.

et al.[13] showed by a reduced-order model approach that increasing the flow index n for a power-law fluid tends to destabilize turbulent points, therefore leading to a delay to turbulence. The focus was made on the centerline velocity without investigating the effective viscosity stratification. The work presented here aims to provide an insight on the radial receptivity of a perturbation along the radial coordinate due to threshold fluid behavior for an HB fluid.

We build on the model of Barkley[11]

$$\dot{q} = -\frac{dV(q)}{dq} \tag{3a}$$

$$V(q) = \frac{q^2}{2}\left[\delta + (\mathcal{R}+\delta)\left(\frac{q^2}{2} - \frac{4q}{3}\right)\right] \tag{3b}$$

$$\left[\frac{\partial q}{\partial t} + (u-\zeta)\frac{\partial q}{\partial z}\right] = q[\mathcal{R} + (u-U_0) - (\mathcal{R}+\delta)(q-1)^2] + D\frac{\partial^2 q}{\partial z^2} \tag{3c}$$

$$\left[\frac{\partial u}{\partial t} + u\frac{\partial u}{\partial z}\right] = \epsilon_1(U_0 - u) + \epsilon_2(\overline{U} - u)q \tag{3d}$$

where the local dynamics of the turbulent kinetic energy is described by (3a), where the potential $V(q)$ is a 4th-degree polynomial defined by (3b), where $\mathcal{R}$ is the normalized Reynolds parameter and δ a fixed constant.

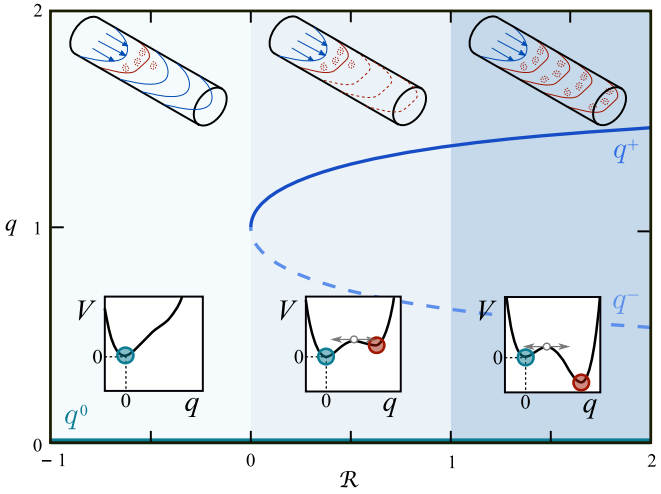

FIG. 2. Bifurcation diagram of the local model dynamics. Three regions are modelled. The corresponding pipe flows are represented on the top and corresponding potentials $V(q)$ are represented on the bottom where filled points are linearly stable states, blue markers denote the laminar state q^0 and red markers denote the turbulent attractors, and white open points are linearly unstable states. In the middle, solid curves indicate linearly stable states and dashed curve indicate unstable states.

The potential term $V(q)$ admits three stationary points q_0, q_+, q_- and, depending on the $\mathcal{R}$ value, three regimes can be identified as shown in fig. 2. The model is made of two constitutive equations, one for the turbulent kinetic energy q (3c) and one for the turbulent velocity u (3d). The model of Barkley[11] was originally proposed for studying intermittency phenomena for a Newtonian fluid and it has been generalized by Romanò et al.[13] to deal with thermal and power-law effects. In this letter, we further generalize the model to deal with an HB fluid (1). To that end, we consider the deformation rate tensor corresponding to an HB fluid and we include the radial derivatives of the background flow $U(r)$ determined a-priori and we neglect the corresponding derivatives of u along r. This hypothesis is motivated for finite-amplitude perturbations $u \ll U$ and allows our reduced-order model to retain the essential non-linear effects required to deal with an HB fluid, yet keeping moderate the complexity of the reduced-order model. We remark that such assumption implies that the flow remains strictly axial, therefore the perturbation does not contribute to the radial derivatives, i.e. $\partial_r u = 0$. Moreover, it allows to study the receptivity of the perturbation to the radial location where it gets triggered. The corresponding modification to the original model consists of replacing the momentum equation (3d) by

$$\begin{aligned}\frac{\partial u}{\partial t} + u\frac{\partial u}{\partial z} =& \frac{1}{r}\frac{\partial}{\partial r}\left\{ r\left[\frac{\mathrm{Hb}}{\mathcal{R}}\left(2\left(\frac{\partial U}{\partial r}\right)^2 + 4\left(\frac{\partial u}{\partial z}\right)^2\right)^{-\frac{1}{2}}\right.\right. \\ &\left.\left. + \frac{1}{\mathcal{R}}\left(2\left(\frac{\partial U}{\partial r}\right)^2 + 4\left(\frac{\partial u}{\partial z}\right)^2\right)^{\frac{n-1}{2}}\right]\frac{\partial U}{\partial r}\right\} \\ &+ 2\frac{\partial}{\partial z}\left\{\left[\frac{\mathrm{Hb}}{\mathcal{R}}\left(2\left(\frac{\partial U}{\partial r}\right)^2 + 4\left(\frac{\partial u}{\partial z}\right)^2\right)^{-\frac{1}{2}}\right.\right. \\ &\left.\left. + \frac{1}{\mathcal{R}}\left(2\left(\frac{\partial U}{\partial r}\right)^2 + 4\left(\frac{\partial u}{\partial z}\right)^2\right)^{\frac{n-1}{2}}\right]\frac{\partial u}{\partial z}\right\} \\ &+ \epsilon_1(U-u) + \epsilon_2(\overline{U}-u)q, \end{aligned} \tag{4}$$

and of replacing U_0 by U in (3c) and (3d). We further stress that replacing (3d) by (4) adds an additional term also for Newtonian flows (Hb=0 and $n = 1$), hence the current model slightly differs from the original version of Barkley[11].

In order to employ (4), we need to determine the velocity profile of the HB flow. This requires the calculation of the size of the unyielded zone, which depends on the rheological properties of the fluid. The size of the unyielded region is here denoted a and is a function of (n,Hb) within the framework of the HB model:

$$\begin{aligned}&(1-a)^{\frac{3n+1}{n}} - \frac{3n+1}{n}(1-a)^{\frac{2n+1}{n}} \\ &+ \frac{(2n+1)(3n+1)}{2n^2}(1-a)^{\frac{n+1}{n}} \\ &+ \frac{(3n+1)(2n+1)(n+1)}{2n^3}\left(\frac{a}{\mathrm{Hb}}\right)^{\frac{1}{n}} = 0 \end{aligned} \tag{5}$$

The background velocity profile is therefore obtained by plugging a in the analytical laminar solution of pipe flow for HB fluids (see Peixinho[20]):

$$U = \begin{cases} \frac{n}{n+1}\left(\frac{\mathrm{Hb}}{a}\right)^{\frac{1}{n}}(1-a)^{\frac{n+1}{n}}, & x \in [0,a) \\ \frac{n}{n+1}\left(\frac{\mathrm{Hb}}{a}\right)^{\frac{1}{n}}\left[(1-a)^{\frac{n+1}{n}} - (x-a)^{\frac{n+1}{n}}\right], & x \in [a,1] \end{cases} \tag{6}$$

The corresponding profiles of a are depicted in fig. 3(a) for varying Hb and n, while fig. 3(b) shows how U varies upon an increase of Hb for $n = 0.7$.

From here on, the results of our model are presented. We remark that the implementation of the original model has already been detailed and validated in a previous work (see Romanò et al.[13]). All the following results are obtained using the same discretization schemes and the same model parameters (δ,ϵ_1,ϵ_2,ζ,$\overline{U}$,c,D) as in Romanò et al.[13]. We here investigate the effects of four parameters: $\mathcal{R}$, n, τ_0 and r, and the corresponding ranges of variation are summarised in tab. I. We fix the turbulence intensity of the initial perturbation and rescale the turbulent velocity to the background flow U, i.e.

$\mathcal{R}$	n	τ_0	r	K	$U_{max}[m \cdot s^{-1}]$	$R[m]$
0.40-1.00	0.70-1.20	0.00-0.90	0.50-0.90	0.10	1.00	1.00
25 values	11 values	10 values	5 absolute+5 relative	-	-	-

TABLE I. Parameters value range in this study. Parameters have been adimensionnalized (n is already adimensionnal). For a detailed analysis about the parameter $\mathcal{R}$ see Barkley (2016)[11].

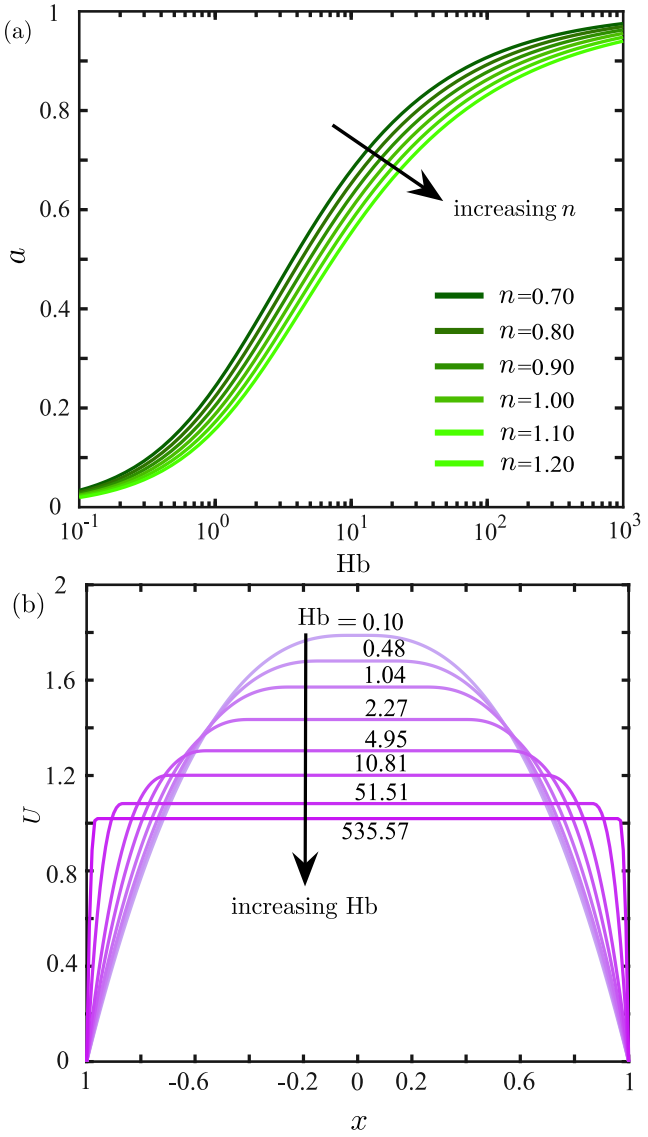

FIG. 3. (a) Iso-velocity zone dimension a with rheological parameters n and Hb. (b) Axial velocity profiles on x positions along the radius axis for $n = 0.7$ upon a change of the Hb values.

$u(t = 0, r) = U(r)$ and $q(t = 0, z) = (0.5 + N(z))$ if $z \in [0.1,\ 0.12]L_{\text{pipe}}$ and $q(t = 0, z) = 0$ elsewhere, with $L_{\text{pipe}} = 1000$ being the pipe length and $N(z)$ a random noise function whose values range within $N(z) \in [0, 0.05]$. The simulations are carried out fixing two out of three parameters (n, τ_0, r) at a time and investigating the dynamics of the system on the planes ($\mathcal{R}$, n), ($\mathcal{R}$, τ_0), and ($\mathcal{R}$, r). The corresponding perturbation at the final simulation time $t_{\text{fin}} = 100$ is depicted in fig. 4 in phase space ($q-u$ coordinates) for every spatial point along the z coordinate. In fig. 4(a) we fix τ_0 and r, and explore the parameter plane ($\mathcal{R}$, n). The case in black considers the fluids described in fig. 1, which is assumed as reference case for the three subfigs. 4(a), (b) and (c). Turbulence is reached at every considered $\mathcal{R} \in \{0.6,\ 0.8,\ 0.96\}$ and the increase in $\mathcal{R}$ results in the corresponding increase of the maximum turbulence level $q_{\max}$. Moreover, when n increases, also $q_{\max}$ tends to increase. The increase of the shear-thickening behavior, i.e. $n \uparrow$, is accompanied by a shift in phase space to lower values of u, meaning puffs and slugs propagate slower for higher value of n, as shown in the space-time graph on the bottom. In fig. 4(b), we fix n and r, and explore the parameter plane ($\mathcal{R}$, τ_0) for $\mathcal{R} \in \{0.6,\ 0.8,\ 0.96\}$. When τ_0 decreases, $q_{\max}$ tends to increase. The increase of the yield stress, i.e. $\tau_0 \uparrow$, is accompanied by a shift in phase space to higher values of u, meaning puffs and slugs propagate faster for higher values of τ_0. Finally, in fig. 4(c) we fix n and τ_0, and move on the parameter plane ($\mathcal{R}$, r) for $\mathcal{R} \in \{0.6,\ 0.8,\ 0.96\}$. Upon an increase of r the maximum turbulence intensity of the perturbation $q_{\max}$ increases. Shifting the inception of the perturbation towards the pipe axis, i.e. $r \downarrow$, is accompanied by a shift in phase space to higher values of u, meaning puffs and slugs propagate slower near the pipe wall and faster near pipe axis, as expected. For low $\mathcal{R}$, the transition to turbulence is only reached when the perturbation is initialized near the wall. For instance, no turbulent stable point exists at $r = (a+1)/2$ for $\mathcal{R} = 0.60$ (case shown in light blue); on the contrary, assuming the same turbulent intensity promotes transition to the turbulent regime at higher r. This is understood considering that the initial perturbation intensity $q(t = 0, z)$ considered so far is constant, hence its importance relative to the background flow increases by shifting the perturbation towards the wall. This may be trivial for Newtonian flows, but is not as self-evident for HB fluids, because the radial derivatives of the background flow profile may potentially play a significant role when $a \to 1$.

Moving on the same three parameter planes considered above, we refine the resolution in $\mathcal{R}$ and focus on $q_{\max}$. A contour plot of $q_{\max}$ on the (r, $\mathcal{R}$)−plane is depicted in fig. 5(b) for (n, τ_0) = (0.7, 0.5). At low $\mathcal{R}$, i.e. $\mathcal{R} \lessapprox 0.6$, $q_{\max}(t = t_{\text{fin}})$ decreased of four to five orders of magnitude with respect to its initial amplitude, meaning that the perturbation at such Reynolds parameters is not strong enough to trigger turbulence in any radial position of the pipe. On the contrary, at $\mathcal{R} = 1$, $q_{\max}$ ranges

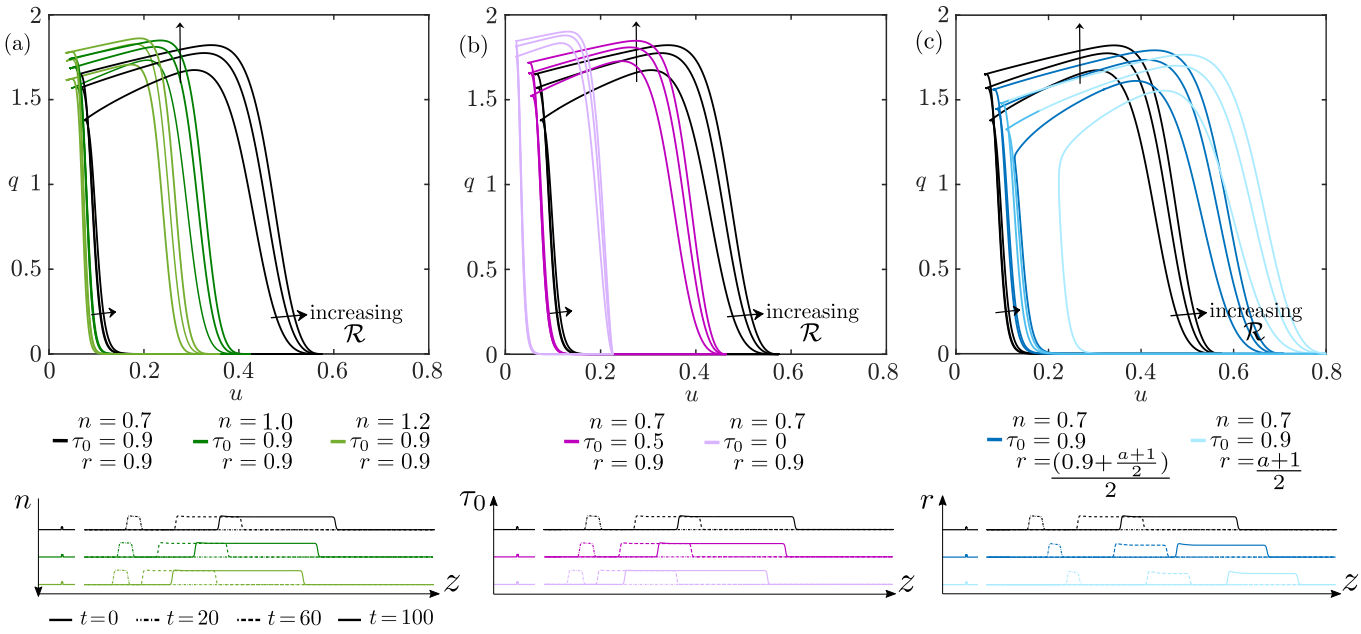

FIG. 4. Three comparisons of q-u phase portrait for each parameter, respectively (a) n, (b) τ_0 and (c) r, for three $\mathcal{R}$ values $(0.60; 0.80; 0.96)$ at final time on the top. The same reference case is plotted in black on the three plots and parameter values are specified under the plots. The corresponding perturbation dynamics for $\mathcal{R} = 0.96$ at different times t are overlaid on parameter versus pipe axis position z graphs on the bottom.

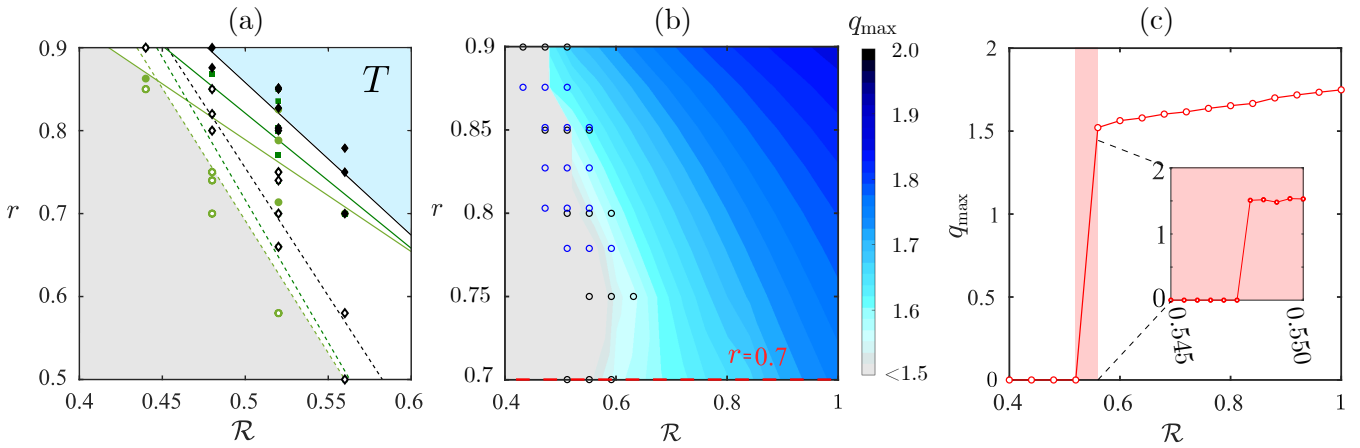

FIG. 5. (a) Transition points from laminar state (L) to turbulent state (T) for different fluid parameters (n, τ_0): $n = 0.7$ (diamond symbols), $n = 1.0$ (square symbols), $n = 1.2$ (circle symbols), open symbols for $\tau_0 = 0$ and full symbols for $\tau_0 = 0.5$. The linear fits of the transition points indicate the edge of the transition for the different fluid parameters. (b) Contour map of $q_{\max}$ on the $(r,\ \mathcal{R})-$plane for $n = 0.7, \tau_0 = 0.5$. This case is depicted in the panel (a) by filled black diamonds. Markers indicate the tested points near the transition, black at the absolute and blue at the relative radial positions. (c) Variation of $q_{\max}$ with $\mathcal{R}$ corresponding to the horizontal dashed red line in (b) for $r = 0.70$. The inset shows a zoom in the transition zone ($\mathcal{R} \sim 0.551$). All the results in this figure consider a perturbation with given initial amplitude A, independently on the radial location where the perturbation is triggered.

from ≈ 1.5 to ≈ 1.7, indicating that the perturbation has grown enough to cause the transition to a stable turbulent point. The radial receptivity to perturbations with the given initial turbulence intensity is inferred from the ordinate of fig. 5(b). Upon an increase of r, the laminar-to-turbulent edge is shifted towards lower $\mathcal{R}$. This is consistent with the observations reported in fig. 4(c), where perturbations triggered near the wall could initiate laminar to turbulent transition at lower Reynolds parameters. Therefore, the contour map in 5(b) defines the radial receptivity of a perturbation with given amplitude for $(n,\ \tau_0) = (0.7,\ 0.5)$. To identify the critical Reynolds parameter $\mathcal{R}_c$, we fixed the radial coordinate r and detect the largest $\mathcal{R}$ such that $q_{\max} < 10^{-5}$ for each ordered pair

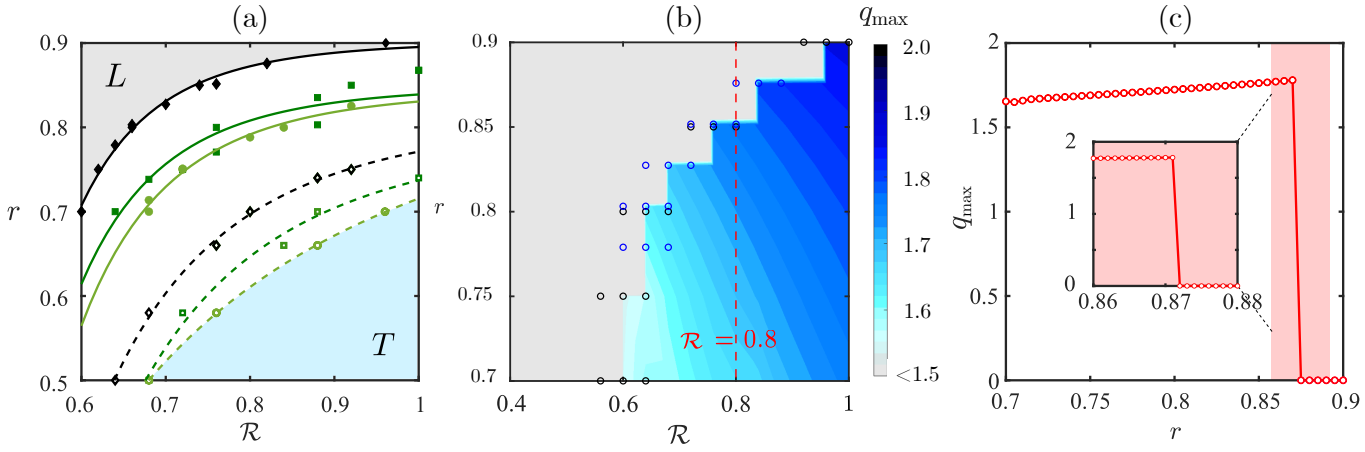

FIG. 6. (a) Transition points from laminar state (L) to turbulent state (T) for the same fluid parameters ($n,\ \tau_0$) as in figure 5. The power-law fits of the transition points indicate the edge of the transition for the same fluid parameters ($n,\ \tau_0$). (b) Contour map of $q_{\max}$ on the ($r,\ \mathcal{R}$)−plane for $n = 0.7, \tau_0 = 0.5$. This case is depicted in the panel (a) by filled black diamonds. Markers indicate the tested points near the transition, black at the absolute and blue at the relative radial positions. (c) Variation of $q_{\max}$ with r corresponding to the vertical dashed red line in (b) for $\mathcal{R} = 0.8$. The inset shows a zoom in the transition zone ($r \sim 0.870$). All the results in this figure consider an initial perturbation normalized with the local background flow $U(r)$ for the r considered to trigger the perturbation.

(n, τ_0). This is demonstrated in fig. 5(c) for $r = 0.7$ (red dashed line in fig. 5(b)). The transition to turbulence predicted by our model is abrupt, as $q_{\max}$ passes from less than 10^{-5} to ≈ 1.5 upon an increment in Reynolds parameter of $\Delta\mathcal{R} = 5 \cdot 10^{-4}$. The inset in fig. 5(c) blows up the neighborhood of the critical Reynolds parameter $\mathcal{R}_c$, showing the sharp transition from the laminar state for $\mathcal{R} = 0.5475$ to the turbulent state at $\mathcal{R} = 0.5480$. This same procedure is carried out for every radial location r with $\Delta r = 0.002$ and each of the six ordered pairs (n, τ_0) described in the 5(a) caption. The laminar-to-turbulent edge is determines for each of these cases on the plane ($r,\ \mathcal{R}$). Corresponding linear fits of the transition lines from laminar (L in fig. 5(a)) to turbulent (T in fig. 5(a)) states are depicted as solid and dotted lines color coded as their respective marker. Figure 5(a) indicates that increasing the yield-stress delays the transition to turbulence to higher $\mathcal{R}_c$. This is in good agreement with the theoretical predictions of Nouar and Frigaard[21] who showed that the yield-stress has a stabilizing effect. Moreover, fig. 5(a) demonstrates that the shear-thinning behavior (black in fig. 5(a)) of an HB fluid tends to delay the transition while shear-thickening triggers turbulence at lower $\mathcal{R}_c$ (light green in fig. 5(a)). Experimental studies (see Bahrani et al.[16] and Peixinho[22]) confirm the behavior predicted by our model, as they find that the transition to turbulence is delayed upon a decrease in n.

Finally, we investigate the effect of a perturbation with a normalized turbulence intensity by carrying out the same analysis presented so far, but for $u(t = 0, r) = U(r)$ and $q(t = 0, z) = (0.5 + N(z))U(r)$ if $z \in [0.1,\ 0.12]L_{\text{pipe}}$ and $q(t = 0, z) = 0$ elsewhere. As we scale the initial turbulence intensity of the perturbation to the background flow, the finite amplitudes near the wall are too small to trigger turbulence, hence the receptivity map admits a pronounced gray area for $r \geq 0.875$ and $(n, \tau_0) = (0.7,\ 0.5)$ (see fig. 6(b)). Similarly to the previous case, also for a normalized perturbation the transition from laminar to turbulence is abrupt in parameter space. This is demonstrated in fig. 6(c) by considering a vertical cut of the parameter plane ($r,\ \mathcal{R}$) at $\mathcal{R} = 0.8$ (see red dashed line fig. 6(b)). The inset in fig. 6(c) shows that turbulence is sustained at $\mathcal{R} = 0.8$ for $r = 0.872$ and it decays for $r = 0.874$. Figure 6(a) depicts the laminar-to-turbulent edge for all the parameters considered in this study employing the same resolution as in fig. 5(a). The transition edges are well fitted by power-laws $(b\mathcal{R}^C + d)$, as demonstrated by the dashed and dotted lines in fig. 6(a). This is due to the enhanced significance of the background flow at large r and to the exponents of the corresponding radial derivatives. In fact, the laminar state tends to diffuse the initial puff thanks to the diffusion term introduced in (4). This is enough to kill an initial small-amplitude puff (normalized initial perturbation). On the contrary, the near-wall puffs studied in fig. 5 are not normalized with $U(r)$, hence their amplitude relative to U increases for $r \to 1$ and it manages to compensate or even to overcome the stabilizing diffusion term. We further remark that an increase in yield stress τ_0 and a decrease in flow index n turn into destabilizing effects for a normalized initial perturbation. This striking change of stabilization character for the rheological parametric ordered pair (n, τ_0) may be due to the growth dynamics of the normalized perturbation, that leads to a more pronounced impact of the terms associated to $\partial_z u$ on the r.h.s. of (4). For a similar case, in fact, Romanò et al.[13] demonstrated that power-law fluids tend to be stabilized by the axial component of the viscous term upon

an increase of n.

To summarize and conclude, in this letter we investigate how the transition to turbulence in a pipe flow is impacted by the rheology of an HB fluid. We generalize the reduced-order model of Barkley[11] to include shear-thinning/-thickening, as well as yield stress effects. We also investigate the receptivity of finite-amplitude perturbations upon a change on the radial position where the perturbation is injected. The typical conditions of an experiment are mimicked by keeping fixed the turbulent intensity of the perturbation and shifting its injection point in radial direction. We find that the presence of a yield-stress and the shear-thinning behavior of an HB fluid tends to stabilize the flow, as also corroborated by the corresponding experiments and the theoretical analyses reported in the literature. Moreover, as the perturbation is not scaled to the local laminar state, the transition to turbulence occurs sooner for perturbations injected near the wall. This is due to the enhanced relative importance of the perturbation amplitude with respect to the background flow. A second investigation has been conducted by rescaling the initial turbulence intensity of the perturbation to the local laminar profile. Our model shows that all the most significant conclusions drawn for a perturbation of given turbulence intensity are reverted when considering a basic-state-normalized $q(t = 0, z)$: (i) the receptivity of the perturbation gets killed by diffusion near the wall, (ii) an increase of yield stress becomes destabilizing, and (iii) an increase of n becomes stabilizing. This last feature was also reported by Romanò et al.[13] for a power-law fluid and explained by emergence of the $|\partial u|^{n-1}$ as a pre-factor that decreases the effective Reynolds number.

DATA AVAILABILITY

The data that support the findings of this study are available from the corresponding author upon reasonable request.

ACKNOWLEDGEMENTS

We gratefully acknowledge funding support from the SIAAP (Greater Paris Sanitation Authority) in the framework of the MOCOPEE French research program and the Hauts-de-France French Region (convention number: 20003867).

AUTHOR DECLARATIONS

The authors have no conflicts to disclose

REFERENCES

[1] Hof, B. et al. 2004 Experimental observation of nonlinear traveling waves in turbulent pipe flow, *Science*, **305**, 1594-1598.
[2] Faisst, H., Eckhardt, B. 2004 Sensitive dependence on initial conditions in transition to turbulence in pipe flow., *J. Fluid Mech.*, **504**, 343-352.
[3] Kerswell, R. R. 2005 Recent progress in understanding the transition to turbulence in a pipe., *Nonlinearity*, **18(6)**, R17.
[4] Avila, K. et al. 2011 The onset of turbulence in pipe flow, *Science*, **333(6039)**, 192-196.
[5] Jiménez, J. 2018 Coherent structures on wall-bounded turbulence , *J. Fluid Mech.*, **842**, P1.
[6] Hof, B., Juel, A., Mullin, T. 2003 Scaling of the turbulence transition threshold in a pipe, *Phys. Rev. Letters*, **91**, 244502.
[7] Peixinho J. 2007 Finite-amplitude thresholds for transition in pipe flow, *J. Fluid Mech.*, **582**, 169-178.
[8] Willis, A.P., Kerswell, R.R. 2007 Critical Behavior in the Relaminarization of Localized Turbulence in Pipe Flow, *Phys. Rev. Letters*, **98**, 014501.
[9] Hof, B. et al. 2008 Repeller or Attractor? Selecting the Dynamical Model for the Onset of Turbulence in Pipe Flow, *Phys. Rev. Letters*, **101**, 214501.
[10] Song, B. et al. 2017 Speed and structure of turbulent fronts in pipe flow, *J. Fluid Mech.*, **813**, 1045–1059.
[11] Barkley, D. 2016 Theoretical perspective on the route to turbulence in a pipe, *J. Fluid Mech.*, **803**, 1-79.
[12] Lemoult, G. et al. 2016 Directed percolation phase transition to sustained turbulence in Couette flow, *Nature Phys.*, **12**, 254–258.
[13] Romanò, F., Charles, A., Dottori, F., Bahrani, S.A. 2021 Transition to turbulence in a heated non-Newtonian pipe flow, *Phys. Fluids*, **33**, 091702.
[14] Coussot, P. 2014 Rheophysics: Matter in all its states, *Springer*, ISBN: 978-3-319-06148-1
[15] Escudier, M.P., Rosa, S., Poole, R.J. 2009 Asymetry in transitional pipe flow of drag-reducing polymer solutions, *J. Non-Newt. Fluid Mech.*,**161**, 19-29.
[16] Bahrani S. A. and Nouar C. 2014 Intermittency in the transition to turbulence for a shear-thinning fluid in Hagen-Poiseuille flow, *J. Appl. Fluid Mech.*, **7**, 1-6.
[17] Virk, P. 1975 Drag reduction fundamentals, *Phys. Fluids*, **21**, 625-656.
[18] Escudier, M.P., Presti, F., Smith, S. 1999 Drag reduction in the turbulent pipe flow of polymers M.P., *J. Non-Newt. Fluid Mech.*,**81**, 197-213.
[19] Chekila, A. 2014 Analyse non linéaire de la stabilité de l'écoulement de Poiseuille plan d'un fluide rhéofluidifiant, PhD. thesis, Univ. Lorraine (France)
[20] Peixinho, J. 2004 Contribution expérimentale à l'étude de la convection thermique en régime laminaire, transitoire et turbulent pour un fluide à seuil en écoulement dans une conduite, PhD. thesis, Univ. Lorraine (France)
[21] Nouar, C., Frigaard, I.A. 2001 Nonlinear stability of Poiseuille flow of a Bingham fluid: theoretical results and comparison with phenomenological criteria, *J. Non-Newtonian Fluid Mech.*, **100**, 127-149.
[22] Peixinho J. 2008 Heat transfer of a non-Newtonian fluid (Carbopol aqueous solution) in transitional pipe flow, *Int. J. of Heat and Mass Transfer*, **51**, 198-209.